Direct single-molecule observation of a protein living in two opposed native structures

Yann Gambin[a,1], Alexander Schug[b,1], Edward A. Lemke[a], Jason J. Lavinder[c,d], Allan Chris M. Ferreon[a], Thomas J. Magliery[c,2], José N. Onuchic[b,2], and Ashok A. Deniz[a,2]

[a]Department of Molecular Biology, The Scripps Research Institute, La Jolla, CA 92037; [b]Center for Theoretical Biological Physics, University of California, San Diego, CA 92093; and [c]Departments of Chemistry and Biochemistry and [d]Ohio State Biochemistry Program, Ohio State University, Columbus, OH 43210

Contributed by José N. Onuchic, April 23, 2009 (sent for review March 23, 2009)

Biological activity in proteins requires them to share the energy landscape for folding and global conformational motions, 2 key determinants of function. Although most structural studies to date have focused on fluctuations around a single structural basin, we directly observe the coexistence of 2 symmetrically opposed conformations for a mutant of the Rop-homodimer (Repressor of Primer) in single-molecule fluorescence resonance energy transfer (smFRET) measurements. We find that mild denaturing conditions can affect the sensitive balance between the conformations, generating an equilibrium ensemble consisting of 2 equally occupied structural basins. Despite the need for large-scale conformational rearrangement, both native structures are dynamically and reversibly adopted for the same paired molecules without separation of the constituent monomers. Such an ability of some proteins or protein complexes to switch between conformations by thermal fluctuations and/or minor environmental changes could be central to their ability to control biological function.

energy landscape theory | protein folding | Rop dimer | single molecule FRET

During the last 2 decades, the advent of energy landscape theory combined with a new generation of experiments have demonstrated that small and intermediate-sized proteins fold in a robust way through an ensemble of converging pathways, a folding funnel, biased toward the native ensemble (1–5). Accordingly, evolutionary pressure forces proteins to have sufficiently reduced energetic frustration that the folding mechanism is dominantly controlled by native interactions, with nonnative contacts being mostly neutral (6, 7). Under the same scenario, some larger and more interesting proteins and protein complexes may achieve more than one conformation while maintaining many native contacts. Examples are conformational substates required for protein function (8, 9), aggregation as in the case of prions (10) and other amyloidogenic proteins (11), changes in multimeric state (12), or domain swapping in protein dimers (13, 14). High structural symmetry has been proposed to be another source of multiple native configurations (15–17). External influences such as changes in the environment or binding to small metabolites may change the protein preference to one of these structures, and therefore may play an important functional role. Earlier studies of the Rop-dimer (Repressor of Primer, also known as ROM) have shown that it can assume different symmetrically-opposed native conformations for the WT (18, 19) and a core-repacked mutant (Ala_2Ile_2-6, called A_2I_2 hereafter) (20). Here, we directly observe by single molecule FRET-measurements the interconversion of a single Rop-mutant sequence between these 2 possible native conformations.

Two monomers, each consisting of a helix–loop–helix motif, self-associate to form the compact 4-helix bundle of the Rop-dimer (see Fig. 1). Early studies on Rop folding were conducted for a collection of sequences including the WT protein and several variants, aimed at optimizing the hydrophobic packing within the dimer (21, 22). These sequences differ in the number and positions of alanine and leucine residues in the "a" and "d" positions of the heptad repeat, effectively repacking the core without perturbing the peripheral residues (Fig. 2) (21).

On the outer surface of the 2 monomers arranged in the *anti* geometry (18, 19), an RNA-binding interface enables the WT-Rop dimer to regulate ColE1 plasmid replication in *Escherichia coli* (23, 24). Surprisingly, specific mutations inside the core of the protein can affect Rop activity. In a dramatic case, the mutant A_2I_2, repacked using hydrophobic isoleucine and alanine residues, "misfolds" into the symmetrically reversed topology (*syn*) that breaks the RNA-binding interface (20) (see Fig. 2*B*).

Overall, mutants that display RNA binding capability have therefore been assumed to possess the interface and *anti* structure of WT-Rop (22, 25). In this article, however, by using single-molecule fluorescence resonance energy transfer (smFRET) to directly monitor conformational distributions, we demonstrate that Rop and its mutants are far more intriguing and observe for each individual dimer the competition of both *syn* and *anti* in a struggle for conformational dominance.

Theoretical considerations supported by computer simulations suggested that a coexisting ensemble of *syn* and *anti* structures explains the anomalies in the kinetic measurements (25) between Rop mutants as a result of a trap door mechanism (16, 17). Aided by theory, we identified the mutant Ala_2Leu_2-6 (called A_2L_2 hereafter) as a good candidate for experimental investigation. By gel-shift assay, this mutant binds RNA with an affinity comparable to the WT (21), has strongly altered folding/unfolding kinetics, and differs from the *syn* A_2I_2 mutant only in 6 isoleucine to leucine mutations per monomer. We thus concentrate on these 3 sequences, WT-Rop and the mutants A_2L_2 and A_2I_2 (Fig. 1).

Results and Discussion

Probing *syn* and *anti* Rop Structures Using Single-Molecule FRET. Single-molecule techniques are powerful tools to investigate structure, dynamics and function of biomolecules while minimizing complications from ensemble averaging (26–33). Single-molecule FRET (smFRET) involves the nonradiative transfer of energy between a donor and an acceptor dye, and its strong distance dependence {with FRET efficiency given by $E_{FRET} = 1/[1 + (R/R_0)^6]$ (26, 34)} provides a molecular ruler for measuring distances in the 30–80 Å range. This long-range distance measurement capability makes it well-suited to directly observe the occupations of different structural basins and monitor the large global changes in geometry between the *syn* and *anti* Rop structures.

Author contributions: Y.G., A.S., J.N.O., and A.A.D. designed research; Y.G. performed research; E.A.L., J.J.L., A.C.M.F., and T.J.M. contributed new reagents/analytic tools; Y.G. and A.S. analyzed data; and Y.G., A.S., T.J.M., J.N.O., and A.A.D. wrote the paper.

The authors declare no conflict of interest.

[1]Y.G. and A.S. contributed equally to this work.

[2]To whom correspondence may be addressed. E-mail: jonuchic@ucsd.edu, magliery@chemistry.ohio-state.edu, or deniz@scripps.edu.

This article contains supporting information online at www.pnas.org/cgi/content/full/0904461106/DCSupplemental.

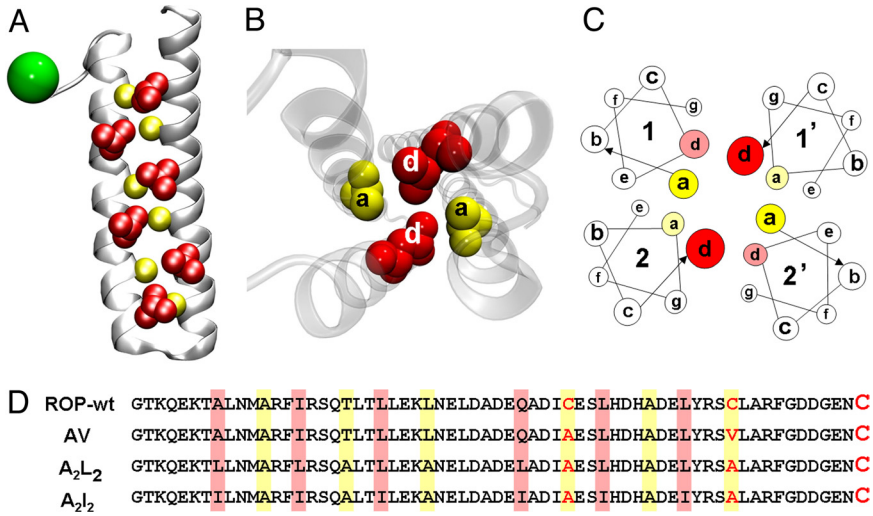

Fig. 1. Monomer structure and heptad repeat of the Rop 4-helix bundle. The only differences between WT-Rop and its mutants Ala_2Leu_2-6 (A_2L_2) and Ala_2Ile_2-6 (A_2I_2) are the inner residues composing the hydrophobic core of the coil-coil. (*A*) As shown for A_2L_2, alanine (yellow) and leucine (red) residues are aligned in 6 layers. (*B* and *C*) The ''a'' and ''d'' residues of the heptad repeats are packed together in the dimer core. (*D*) Sequences of the Rop variants used in this work. The AV-mutant is used as a control for the WT to eliminate possible artifacts from labeling buried cysteine residues (see *SI Text* and Figs. S1 and S2).

To prepare proteins for FRET measurements, for each Rop variant (WT, A_2L_2, and A_2I_2), samples were separately labeled with either Alexa Fluor 488 (donor) or Alexa Fluor 647 (acceptor) dyes at the C-terminal cysteines. Labeling was performed under folding conditions, i.e., on dimeric Rop, to prevent dye access to internal cysteines in WT Rop (Figs. S1 and S2). After unfolding and dimer dissociation in guanidinium chloride (GdmCl), donor and acceptor-labeled monomers were combined and refolded to form the FRET dimer. This procedure yields a mixture of donor–donor-, donor–acceptor-, and acceptor–acceptor-labeled dimers; as a result, ensemble FRET values would be difficult to interpret and unlikely to show conclusive structural evidence.

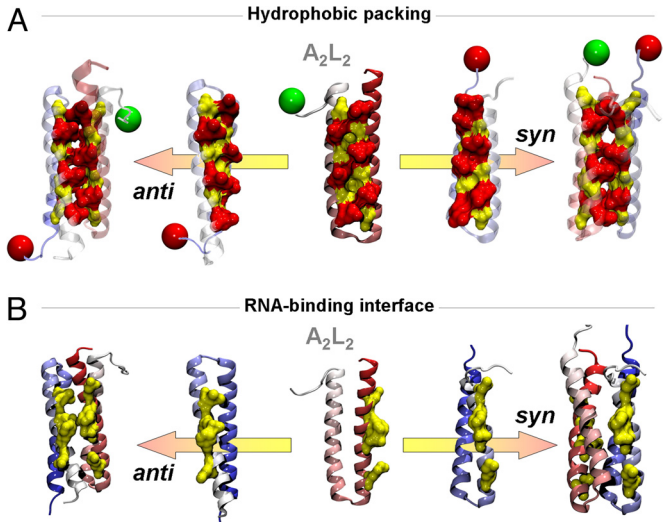

Fig. 2. Schematic of *anti* (*Left*) and *syn* (*Right*) dimer assembly for the A_2L_2 mutant, leading to an active (*anti*) or inactive (*syn*) Rop-dimer. (*A*) For the repacked Rop-variants, the mutations have created a near symmetry of the molecule. This symmetry opens the possibility of 2 opposite geometries: The 2 monomers can bind in a *syn* or in an *anti* conformation (16, 17). The FRET-dyes (indicated as green and red large spheres) are attached to the C termini and have significantly different interdye spatial distances in the 2 states. Thus, smFRET experiments can readily distinguish between the 2 conformations. Both conformations lead to a very similar packing of the alanine and leucine/isoleucine residues within the hydrophobic core, as indicated by the red and yellow surfaces representing the innermost 2 layers. (*B*) However, the structural rearrangement has a direct impact on Rop-dimer functionality: The RNA-binding interface (yellow) is formed on the combined surface of each monomer's first helix, only when the 2 monomers are in the *anti* geometry (18, 19).

We thus performed single-molecule FRET experiments to examine structural distributions, while focusing solely on the donor–acceptor FRET pairs formed by Rop dimers. First, Rop dimers were dispersed in native buffer at a low concentration (≈100 pM) enabling observation of individual dimers by smFRET, in a ''freely-diffusing'' format (35, 36). In these experiments, laser excitation of the donor dye and simultaneous detection of donor and acceptor fluorescence were performed using a high numerical aperture objective and confocal detection. When molecules diffuse through the focal volume, emitted bursts of fluorescence from the donor and acceptor dyes are separately and simultaneously recorded by high-efficiency avalanche photodiodes. The series of such bursts in a time-trajectory were then analyzed to produce histograms of FRET efficiency (E_{FRET}), which contain information about distance, structural populations and distributions (26, 37, 38) (see *SI Text*). Examination of the WT Rop smFRET histograms showed a single FRET peak centered at E_{FRET}≈0.45 (Fig. 3*A*). We then performed similar experiments with the A_2I_2 mutant and obtained histograms with a FRET peak at ≈0.75 (Fig. 3*C*).

These results are consistent with the expected *anti* and *syn* structures respectively, which place the donor/acceptor dyes further or closer to each other (Fig. 1). We note that the major source of the observed peak-broadening is experimental shot-noise, in addition to other contributions (35, 36). Having documented the smFRET signatures for the *anti* and *syn* Rop geometries, using the well-characterized WT and A_2I_2 variants as references, we next examined the A_2L_2 mutant.

The Active State Is Not the Major Structure for A_2L_2 Rop Under Native Conditions, and the *syn*/*anti* Balance Is Altered by Mild Denaturation. Because the A_2L_2 mutant binds RNA with a similar affinity as the WT, it is believed to adopt the same *anti* structure (21).

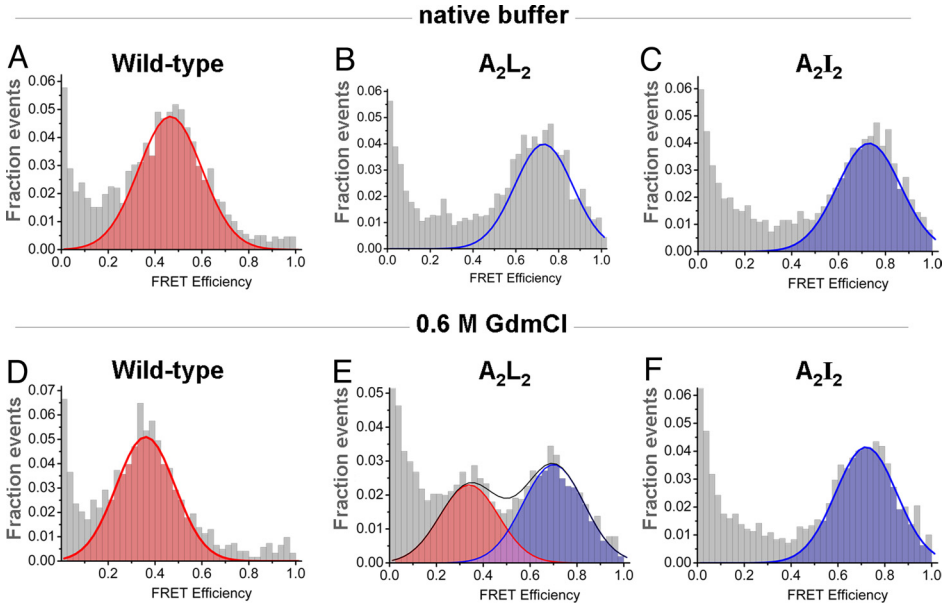

Fig. 3. Single-molecule FRET histograms for Rop and its mutants obtained in native buffer (*A–C*) and in slightly denaturing conditions, 0.6 M GdmCl (*D–F*). The distance between the labeling sites is ≈40 Å in the *anti* and ≈20Å in the *syn* conformation. (*A* and *C*) Because the FRET-efficiency is inversely linked to the distance between the donor and the acceptor, the peaks at $E_{FRET} = 0.45$ (*A*) and ≈0.75 (*C*) are related to Rop being in the *anti* and *syn* conformations respectively. The gray bars give the data with red (*anti*) and blue (*syn*) showing Gaussian fits to them. (*D*) We conclude that the WT stays in *anti*, although the peak shifts slightly to lower FRET-efficiencies for higher concentrations of GdmCl. (*F*) This relative shift could be due to variations in dyes properties, or possibly small effects on local structures. The mutant A_2I_2 stays clearly in *syn*, because the FRET peaks remains at a stable value. (*B* and *E*) For the mutant A_2L_2, we observe an occupation of *syn* for 0 M denaturant (*B*) (see also Fig. S3) and a mixed ensemble of *syn*/*anti* states at 0.6 M GdmCl (*E*) (see also the control experiment Fig. S4).

Surprisingly, when we carried out smFRET experiments on this variant, we discovered that the histogram observed closely matches the one obtained for the A_2I_2 mutant, with a peak at high-E_{FRET} (Fig. 3*B*; see Fig. S3 for overlay). Based on the previous peak assignments, this result clearly demonstrates that the A_2L_2 adopts a *syn* arrangement in native buffer. To further investigate the energetic balance between the 2 structures, we next explored the denaturation behavior of the Rop variants.

Earlier studies using simulations (16, 17) showed that the *syn* and *anti* geometries lead to dissimilar kinetic and folding behavior. One might therefore envision the possibility that the 2 structures are differentially affected by denaturant. To probe the stability of the Rop dimers, using smFRET, we performed a titration with the denaturant guanidinium chloride (GdmCl). WT and A_2I_2 both maintain their single FRET peaks up to GdmCl concentrations of 5 and 4 M respectively, where complete loss of the FRET peak suggests rapid dimer-dissociation. In contrast, A_2L_2 has strikingly different behavior: A second peak appears at $E_{FRET} \approx 0.35$ in addition to the original peak at $E_{FRET} \approx 0.7$ in the FRET histograms at slightly denaturing conditions (Fig. 3*E*). Additionally, dissociation at single molecule concentrations occurs at a much lower concentration of denaturant (1 M GdmCl). The 2 peaks closely match the ones observed for the reference WT and A_2I_2 (Fig. 3 *D* and *F*).

Indeed, a very similar histogram could be obtained when WT and A_2I_2 were mixed together (see Fig. S4). Hence, the balance between the *syn* and *anti* structures can be tuned by the denaturant concentration, and an equal population was reached ≈0.6 M GdmCl. These data demonstrate that although A_2L_2 folds predominantly into the *syn* geometry under native conditions, the population balance can be dramatically shifted with mild perturbations (Fig. 5*B*). Computer simulations show that rmsd-fluctuations of these 3 mutants around the syn and anti conformations differ (16). For the WT, the *anti* conformation fluctuates less; for A_2I_2 *syn* and for A_2L_2 both conformations fluctuated comparably. This indicates that details of packing are likely responsible for the dissimilar behavior of the mutants.

Two peaks can be distinguished in the histograms obtained for A_2L_2, which reveals that the structural interconversions between *syn* and *anti* structures occur at timescales significantly greater than the approximately millisecond observation time.

Do Transitions Between *syn* and *anti* Structures Occur Intermolecularly or Intramolecularly? Given these intriguing observations, we still need to answer the following question: Does A_2L_2 switch predominantly between the *syn* and *anti* basins by initial dissociation of *syn* dimer followed by recombination of the monomers, or does this switch occur directly in each individual dimer without the need for dissociation? To distinguish between these possibilities, we performed 3-color smFRET experiments as depicted in Fig. 4.

We started with a mixture of A_2L_2-monomers in native buffer labeled with either Alexa Fluor 488 or Alexa Fluor 647 and formed stable dimers in the *syn* structure. We then diluted the proteins rapidly within a slightly denaturing solution of 0.45 M GdmCl (conditions resulting in a mixture of *syn* and *anti* states), containing a large excess (up to 300-fold) of monomers labeled with a third dye, Alexa Fluor 594. If the *syn* Rop-dimer needs to dissociate into monomers to form the *anti* conformation, the Alexa Fluor 647-labeled monomers should be replaced by the excess of competing Alexa Fluor 594-labeled monomer. Using the same experimental setup, because FRET between the Alexa Fluor 488-Alexa Fluor 594 dye-pair is higher for both *syn* and *anti* states (see Fig. S5), we should observe in that case a transfer toward a higher-FRET peak. This was indeed observed in the control experiment shown in Fig. 4*C*. Instead, the resulting histograms in Fig. 4*B* are very similar to those obtained in the 2-color smFRET experiment, clearly demonstrating that there is no substantial exchange of

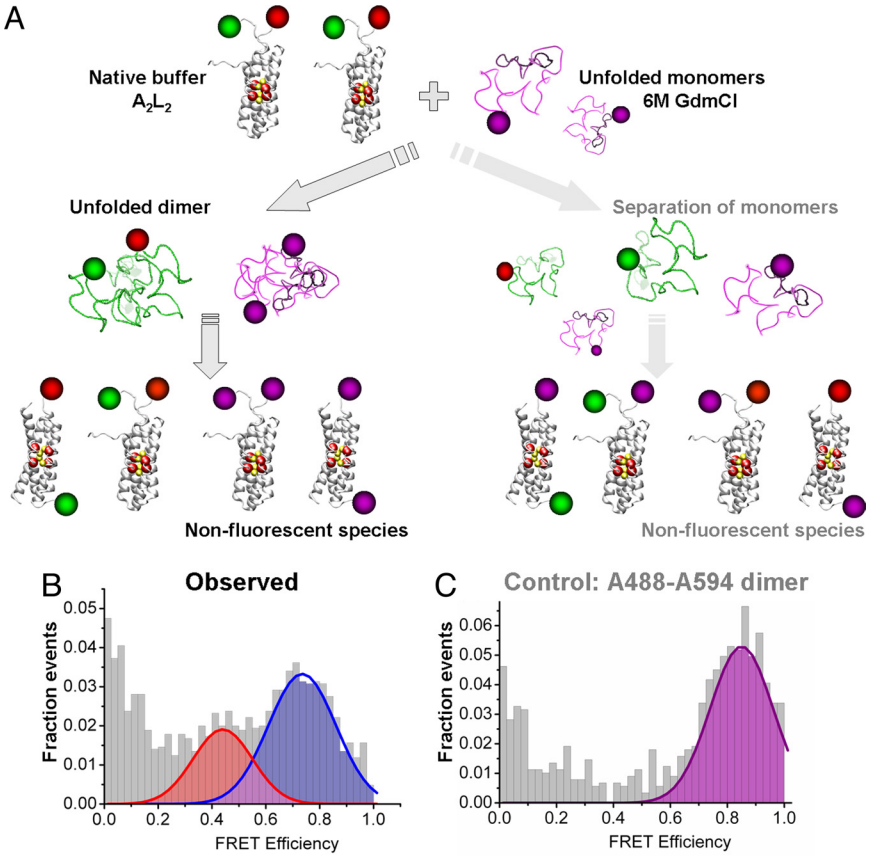

Fig. 4. 3-color FRET-measurements test separation of monomers during conformational transitions. (*A*) Initially, the A_2L_2 dimers labeled with Alexa Fluor 488 (green) and Alexa Fluor 647 (red) are formed in native buffer (0 M GdmCl), favoring the *syn* conformation. We add a 100- to 300-fold higher concentration of unfolded A_2L_2 monomers labeled with Alexa Fluor 594 (purple) and simultaneously change the GdmCl concentration of the mixture to 0.45 M. This triggers conformational transitions from the *syn* to the *anti* structure. The 2 hypotheses (''separation of monomers'' or ''rearrangement within dimer'') would lead to different mixtures of donor–acceptor pairs, fluorescent and nonfluorescent species. As described in Fig. S5, using the same 2 donor and acceptor detection channels, these smFRET measurements can easily detect if Alexa Fluor 488 labeled monomers have separated and reassembled with Alexa Fluor 594 monomers. (*C*) For complete separation of monomers, a shifted peak ≈0.85 should be observed, as obtained in the control experiment where A488, A594, and A647 monomers are mixed in 6 M GdmCl before refolding to similar conditions (0.45 M GdmCl). (*B*) Because the FRET populations obtained after mixing match the original data, we conclude that the *syn*-to-*anti* transition occurs intramolecularly without A_2L_2 dimer dissociation.

monomers during the *syn-anti* conformational transition and no higher-order multimers are adopted. We conclude that despite the large-scale conformational change required, the Rop dimer can switch between the 2 structural basins without monomer exchange or change in oligomeric state (Fig. 4).

Overall, a key result from this work is the striking observation that native A_2L_2 adopts the *syn* conformation, which does not possess the RNA-binding interface, even though A_2L_2 has an in vitro RNA-binding affinity comparable to the WT (22, 25), and an in vivo screen that links Rop function to GFP expression demonstrates that A_2L_2 is functional in *E. coli*, whereas A_2I_2 is not (39) (Fig. 5). The low stability of A_2L_2 together with its tunable ability to interconvert between *syn* and *anti* conformations provide new insight into these apparently conflicting observations of a predominantly inactive *syn* conformation with the ability to bind RNA. The results suggest a possible mechanism in which RNA binds to the molecules in the alternative *anti* structural basin, shifting the dimer equilibrium toward Rop's active conformation, thereby creating the functional population observed in vivo and in vitro. Although the full Rop-dimer—RNA kissing loop quaternary complex has micromolar dissociation constants making detailed single-molecule observation more involved, ongoing developments in fast dilution techniques combined with multicolor smFRET will soon permit direct monitoring of the complete landscape for the coupled Rop-RNA binding and folding.

Our data are also in accord with computational predictions about the properties of core-repacked Rop variants, which suggested that slow folding kinetics might be the result of topological homogeneity, whereas faster kinetics result from structural heterogeneity (16, 17). We confirmed that the unfolding rate of A_2L_2 is much faster than WT [estimated to be 30,000× faster (25)].

Herein, we have used the strength of single molecule detection (26, 33, 40) to directly evaluate the distribution of molecular states in the Rop dimer system, and discover an interconversion between *anti* (active) and *syn* (inactive) native structures. More generally, other proteins might also possess conformations on the verge of structural heterogeneity and express a behavior similar to Rop (41). The balance between multiple competing structural basins would be affected by amino acid mutations, and could even be dynamically altered by changing environmental conditions such as concentration of particular ions or other small molecules, and changes in temperature or pH. It seems quite plausible that living systems exploit such a conformational competition as a regulatory mechanism, for example by modulating binding to specific partners or by tuning protein activity during cellular processes.

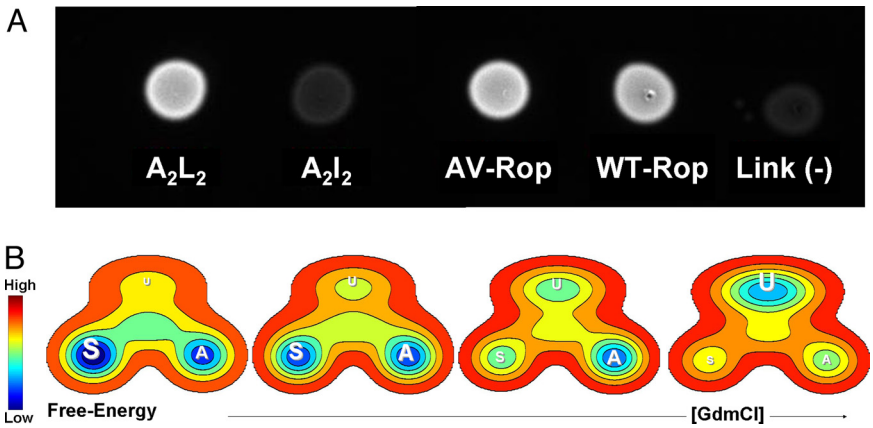

Fig. 5. Rop activity and schematic free-energy landscape of A_2L_2. (*A*) A well-developed in vivo GFP screen for Rop activity shows that the A_2L_2 repacked variant is active whereas the A_2I_2 variant is inactive as compared with the positive and negative controls. The screen monitors the plasmid level of a ColE1 vector with a reporter GFP. In this case, the format of the screen is such that high levels of fluorescence indicate low levels of the ColE1 reporter plasmid and thus an active Rop variant. The link negative control is the empty p15A plasmid (pACT7lac-Cm) on which we have cloned the other Rop variants. This screen requires that the cells be grown at 42 °C to attain runaway plasmid replication of the ColE1 plasmid (for a negative phenotype). (*B*) Schematics of the free-energy landscape of A_2L_2 for different denaturant concentrations. For changing denaturant concentration, the free-energy landscape changes and the 3 states *Anti* (A), *Syn* (S), and Unfolded (U) get populated accordingly (left to right: 0, 0.6, 1, and 2 M GdmCl). When no denaturant is present, the *Syn* and *Anti* basins are respectively strongly and weakly populated, whereas the unfolded ensemble is not adopted. For 0.6 M GdmCl, *Syn* and *Anti* are equally populated and transitions between the 2 states occur directly without disassociation of the monomers composing the dimer. Under unfolding concentrations >1.5 M GdmCl, *Syn* and *Anti* are energetically disfavored and the separated monomers (U) becomes the dominant part of the energy landscape.

Materials and Methods

Preparation and Dual-Labeling of Rop Dimers. Expression and purification of WT and mutant Rop proteins were carried out following procedures described in refs. 20–22 and 25. The final (or measurement) buffer is 200 mM NaCl, 100 mM Tris, pH 8.0

For protein labeling, Rop C-terminal cys mutants were reacted with Alexa Fluor 488 maleimide (donor), Alexa Fluor 594 maleimide (acceptor 1) or Alexa Fluor 647 maleimide (acceptor 2) dyes (Molecular Probes) in 6 M guanidine hydrochloride (GdmCl), 100 mM Tris, pH 7.2, 4 °C, overnight and in the dark. The mono-labeled proteins were subsequently purified from the unlabeled dyes, using NAP columns (GE Healthcare) or Microcon Centrifugal devices (Millipore); the identity and purity of the reaction products were verified by ESI-MS mass spectrometry (Scripps Center for Mass Spectrometry).

For WT Rop at the C-terminal cys, the protein was labeled separately under folding conditions (200 mM NaCl, 100 mM Tris, pH 7.2) to protect the internal cysteines from the reactive dyes (see Figs. S1 and S2). The AV mutant, with internal cysteines removed by mutation, produces the same FRET histograms as the WT labeled under folding conditions. This verifies that <5% of the measured WT dimers would present mislabeling of the internal cysteines. The WT is the most stable structure of the constructs investigated here, because its unfolding occurs in no less than a day in 6 M GdmCl. In comparison, the labeling reaction itself is complete on a much shorter timescale (1 h), consistent with the nondetectable internal labeling. Moreover, our study shows that the formation and stability of the Rop-dimers is extremely sensitive to packing effects within the hydrophobic core. If any dye was present on the hydrophobic surface of a WT monomer, it would perturb deeply the binding interface and likely prevent the formation of the dimer. As a result, these mislabeled WT proteins would not create FRET pairs and would not be detected in our experiments. We thus conclude that the FRET events detected in our single molecule experiments correspond to WT-Rop where the exposed terminal cysteines were predominantly labeled by our protocol.

Single-Molecule FRET Measurements and Analysis. Single-molecule FRET measurements were performed as described in refs. 26, 34, 35, and 42 (see additional details in *SI Text*). Briefly, the FRET efficiency histograms described in this article were generated by using a 2-channel data collection mode to simultaneously record donor and acceptor signals as a function of time, with a binning time of 500 μs. The donor–acceptor solutions used were $\approx$100 pM in fluorophore concentration, ensuring that virtually all of the detected signals were due to single molecules.

The background counts, leakage of donor into the acceptor channel and direct excitation of acceptor were estimated in separate experiments, and used to correct the signals before FRET analysis. A threshold of 50 counts (the sum of signals from the 2 channels) was then used to separate fluorescence signals from background, and FRET efficiencies were calculated for each accepted event and plotted in the form of a histogram.

The FRET-efficiency histograms were fitted with Gaussian functions, using Origin (OriginLab) and IGOR (WaveMetrics) softwares, and the peak positions and areas obtained from the fitting parameters. At least 8 measurements were made for each sample to construct a FRET histogram. FRET efficiencies are defined on the basis of the corrected donor (I_D) and acceptor (I_A) fluorescence intensities as

$$E_{FRET} = \frac{I_A}{I_A + \gamma I_D} \quad [1]$$

where γ is a correction factor dependent on the donor (Φ_D) and acceptor (Φ_A) quantum yields, and donor channel (η_D) and acceptor channel (η_A) detection efficiencies as follows:

$$\gamma = \frac{\eta_A \Phi_A}{\eta_D \Phi_D} \quad [2]$$

γ is known from previous measurements to be close to 1 (42, 43) and is assumed to be constant at 1 for the purpose of this article. This is a reasonable assumption because we do not use absolute distances to make conclusions in our article, and the dye labels on the floppy C termini are in very similar environments for *syn* and *anti* conformations (hence, dye quantum yields in the 2 states are expected to be the same).

Rather than use absolute distance measurements, we use standards to assign states corresponding to the FRET peaks for the A_2L_2. For each condition, we compare the histograms obtained for A_2L_2 to the one obtained for WT-Rop and A_2I_2. Because the crystal structure have been determined for these 2 dimers respectively in the *anti* and *syn* conformations, and the relative distance changes for the FRET peaks are consistent with these 2 structures, we use them as references to determine the conformation(s) adopted by the A_2L_2 variant (see Figs. S3 and S4).

ACKNOWLEDGMENTS. We are grateful to E. Sierecki (University of California at San Diego) for helping in the protein purification and expression. This work was supported by National Institutes of Health Grants GM066833 and GM083114, National Science Foundation Grants MCB-0543906 and PHY-0750049, the Center for Theoretical Biological Physics (which is sponsored by the National Science Foundation) Grant PHY-0822283, a La Jolla Interface in Science Program postdoctoral fellowship (to Y.G.), a Great Rivers Affiliate of the American Heart Association predoctoral fellowship (to J.J.L.), and a National Institute of Neurological Disorders and Stroke/National Institutes of Health postdoctoral fellowship (to A.C.M.F.).

1. Frauenfelder H, Sligar SG, Wolynes PG (1991) The energy landscapes and motions of proteins. *Science* 254:1598–1603.
2. Leopold PE, Montal M, Onuchic JN (1992) Protein folding funnels—a kinetic approach to the sequence structure relationship. *Proc Natl Acad Sci USA* 89:8721–8725.
3. Bryngelson JD, Onuchic JN, Socci ND, Wolynes PG (1995) Funnels, pathways, and the energy landscape of protein-folding—a synthesis. *Proteins* 21:167–195.
4. Onuchic JN, Luthey-Schulten Z, Wolynes PG (1997) Theory of protein folding: The energy landscape perspective. *Annu Rev Phys Chem* 48:545–600.
5. Snow CD, Nguyen N, Pande VS, Gruebele M (2002) Absolute comparison of simulated and experimental protein-folding dynamics. *Nature* 420:102–106.
6. Dill KA, Ozkan SB, Shell MS, Weikl TR (2008) The protein folding problem. *Annu Rev Biophys* 37:289–316.
7. Onuchic JN, Wolynes PG (2004) Theory of protein folding. *Curr Opin Struct Bio* 14:70–75.
8. Best RB, Chen YG, Hummer G (2005) Slow protein conformational dynamics from multiple experimental structures: The helix/sheet transition of arc repressor. *Structure* 13:1755–1763.
9. Okazaki K, Koga N, Takada S, Onuchic JN, Wolynes PG (2006) Multiple-basin energy landscapes for large-amplitude conformational motions of proteins: Structure-based molecular dynamics simulations. *Proc Natl Acad Sci USA* 103:11844–11849.
10. Dima RI, Thirumalai D (2004) Probing the instabilities in the dynamics of helical fragments from mouse PrPc. *Proc Natl Acad Sci USA* 101:15335–15340.
11. Yu JP, Malkova S, Lyubchenko YL (2008) α-Synuclein misfolding: Single molecule AFM force spectroscopy study. *J Mol Biol* 384:992–1001.
12. Tuinstra RL, et al. (2008) Interconversion between two unrelated protein folds in the lymphotactin native state. *Proc Natl Acad Sci USA* 105:5057–5062.
13. Yang SC, et al. (2004) Domain swapping is a consequence of minimal frustration. *Proc Natl Acad Sci USA* 101:13786–13791.
14. Bennett MJ, Choe S, Eisenberg D (1994) Domain swapping—entagling alliances between proteins. *Proc Natl Acad Sci USA* 91:3127–3131.
15. Wolynes PG (1996) Symmetry and the energy landscapes of biomolecules. *Proc Natl Acad Sci USA* 14249–14255.
16. Levy Y, Cho SS, Shen T, Onuchic JN, Wolynes PG (2005) Symmetry and frustration in protein energy landscapes: A near degeneracy resolves the Rop dimer-folding mystery. *Proc Natl Acad Sci USA* 102:2373–2378.
17. Schug A, Whitford PC, Levy Y, Onuchic JN (2007) Mutations as trapdoors to two competing native conformations of the Rop-dimer. *Proc Natl Acad Sci USA* 104:17674–17679.
18. Banner DW, Cesareni G, Tsernoglou D (1983) Crystallization of the ColE1 ROP protein. *J Mol Biol* 170:1059–1060.
19. Banner DW, Kokkinidis M, Tsernoglou D (1987) Structure of the ColE1 ROP protein a 1.7 A resolution. *J Mol Biol* 196:657–675.
20. Willis MA, Bishop B, Regan L, Brunger AT (2000) Dramatic structural and thermodynamic consequences of repacking a protein's hydrophobic core. *Structure* 8:1319–1328.
21. Munson M, Obrien R, Sturtevant JM, Regan L (1994) Redesigning the hydrophobic core of a 4-helix bundle protein. *Protein Sci* 3:2015–2022.
22. Munson M, et al. (1996) What makes a protein a protein? Hydrophobic core designs that specify stability and structural properties. *Protein Sci* 5:1584–1593.
23. Cesareni G, Muesing MA, Polisky B (1982) Control of ColE1 DNA-replication—The ROP gene-product negaticely affects transcription from the replication primer promoter. *Proc Natl Acad Sci USA* 79:6313–6317.
24. Tomizawa J, Som T (1984) Control of ColE1 plasmid replication—Enhancement of binding of RNA-I to the primer transcript by the ROM protein. *Cell* 38:871–878.
25. Munson M, Anderson KS, Regan L (1997) Speeding up protein folding: Mutations that increase the rate at which Rop folds and unfolds by over four orders of magnitude. *Fold Design* 2:77–87.
26. Deniz AA, Mukhopadhyay S, Lemke EA (2008) Single-molecule biophysics: At the interface of biology, physics and chemistry. *J R Soc Interface* 5:15–45.
27. Aleman EA, Lamichhane R, Rueda D (2008) Exploring RNA folding one molecule at a time. *Curr Opin Chem Biol* 12:647–654.
28. Dudko OK, Hummer G, Szabo A (2008) Theory, analysis, and interpretation of single-molecule force spectroscopy experiments. *Proc Natl Acad Sci USA* 105:15755–15760.
29. Joo C, Balci H, Ishitsuka Y, Buranachai C, Ha T (2008) Advances in single-molecule fluorescence methods for molecular biology. *Annu Rev Biochem* 77:51–76.
30. Karymov MA, Bogdanov A, Lyubchenko YL (2008) Single molecule fluorescence analysis of branch migration of Holliday junctions: Effect of DNA sequence. *Biophys J* 95:1239–1247.
31. Mickler M, et al. (2007) Revealing the bifurcation in the unfolding pathways of GFP by using single-molecule experiments and simulations. *Proc Natl Acad Sci USA* 104:20268–20273.
32. Steiner M, Karunatilaka KS, Sigel RKO, Rueda D (2008) Single-molecule studies of group II intron ribozymes (vol 105, art no 13853, 2008). *Proc Natl Acad Sci USA* 105:18071.
33. Cornish PV, Ha T (2007) A survey of single-molecule techniques in chemical biology. *ACS Chem Biol* 2:53–61.
34. Deniz AA, et al. (2001) Ratiometric single-molecule studies of freely diffusing biomolecules. *Annu Rev Phys Chem* 52:233–253.
35. Deniz AA, et al. (1999) Single-pair fluorescence resonance energy transfer on freely diffusing molecules: Observation of Forster distance dependence and subpopulations. *Proc Natl Acad Sci USA* 96:3670–3675.
36. Deniz AA, et al. (2000) Single-molecule protein folding: Diffusion fluorescence resonance energy transfer studies of the denaturation of chymotrypsin inhibitor 2. *Proc Natl Acad Sci USA* 97:5179–5184.
37. Michalet X, Weiss S, Jager M (2006) Single-molecule fluorescence studies of protein folding and conformational dynamics. *Chem Rev* 106:1785–1813.
38. Schuler B, Eaton WA (2008) Protein folding studied by single-molecule FRET. *Curr Opin Struct Biol* 18:16–26.
39. Magliery TJ, Regan L (2004) A cell-based screen for function of the four-helix bundle protein Rop: A new tool for combinatorial experiments in biophysics. *Protein Eng Des Sel* 17:77–83.
40. Karymov M, Daniel D, Sankey OF, Lyubchenko YL (2005) Holliday junction dynamics and branch migration: Single-molecule analysis. *Proc Natl Acad Sci USA* 102:8186–8191.
41. Yadav MK, et al. (2006) Coiled coils at the edge of configurational heterogeneity. Structural analyses of parallel and antiparallel homotetrameric coiled coils reveal configurational sensitivity to a single solvent-exposed amino acid substitution. *Biochemistry* 45:4463–4473.
42. Ferreon ACM, Gambin Y, Lemke EA, Deniz AA (2009) Interplay of α-synuclein binding and conformational switching probed by single-molecule fluorescence. *Proc Natl Acad Sci USA* 106:5645–5650.
43. Mukhopadhyay S, Krishnan R, Lemke EA, Lindquist S, Deniz AA (2007) A natively unfolded yeast prion monomer adopts an ensemble of collapsed and rapidly fluctuating structures. *Proc Natl Acad Sci USA* 104:2649–2654.

Supporting Information

Gambin et al. 10.1073/pnas.0904461106

SI Materials and Methods: Single-Molecule FRET Experiments

Single molecule FRET experiments were carried out on a home built laser confocal microscope system, using an Axiovert 200 microscope (Zeiss). Excitation was achieved by focusing the 488 nm line of a 543-AP-A01 tunable argon-ion laser (Melles Griot) inside the sample solution, 30 μm from the glass cover-slip surface, using a water immersion objective (1.2 NA, 63×; Zeiss). The fluorescence emission was collected using the same objective, separated from the excitation light, using a dichroic mirror (Q495LP; Chroma Tech), spatially filtered using a 100 μm pinhole, then separated into donor and acceptor components using a second dichroic mirror (560 DCXR; Chroma). The donor and acceptor signals (I_D and I_A) were further filtered using an HQ 525/50M band-pass filter (donor; Chroma) and a 590 LPV2 long-pass filter (acceptor; Chroma), then detected using SPCM-AQR-14 avalanche photodiode (APD) photon counting modules (Perkin-Elmer Optoelectronics). Photon counts were recorded using a photon counting card (PCI 6602, National Instruments) interfaced with a computer. Data analysis was performed as described in *Materials and Methods*.

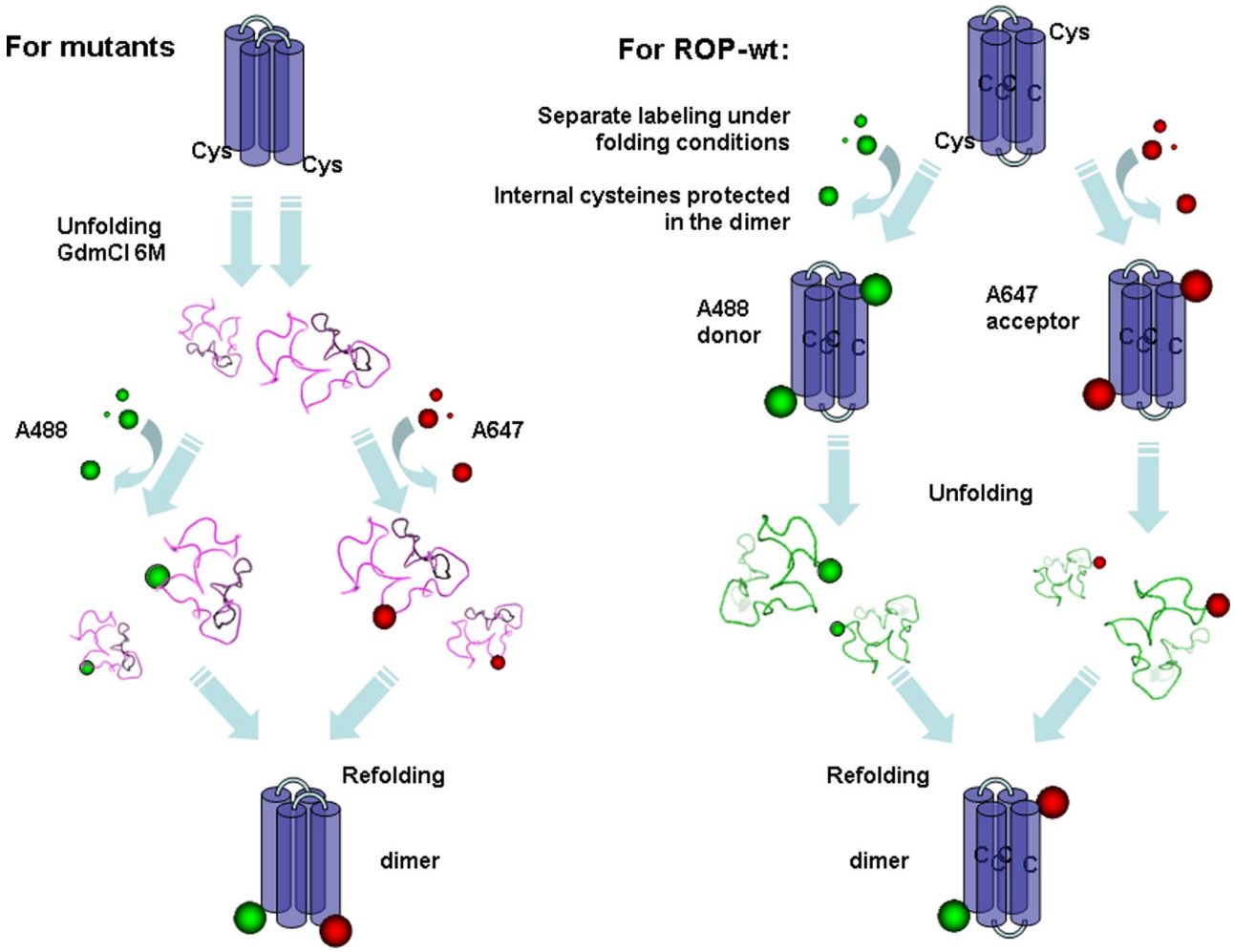

Fig. S1. Schematic of the WT and mutant dual-labeling strategies. The A_2L_2, A_2I_2, or AV mutants can be labeled in denaturant, whereas the WT-Rop is labeled under folding conditions. See main text for details.

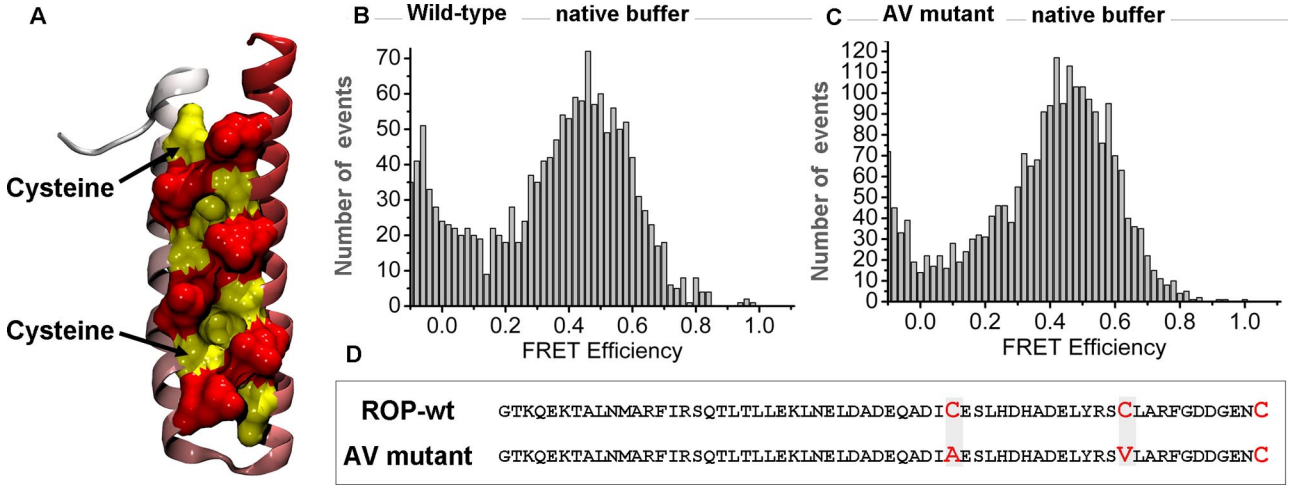

Fig. S2. Protection of internal cysteines of Rop WT by dimerization. (*A*) Schematic of the WT Rop monomer, displaying the two internal cysteines that are buried in the hydrophobic core when the dimer forms. (*B* and *C*) Comparison of the histograms obtained for WT Rop and the AV mutant in native buffer confirms that the exposed WT cysteines are predominantly labeled using our protocol. (*D*) Sequences of the WT Rop and of the AV mutant.

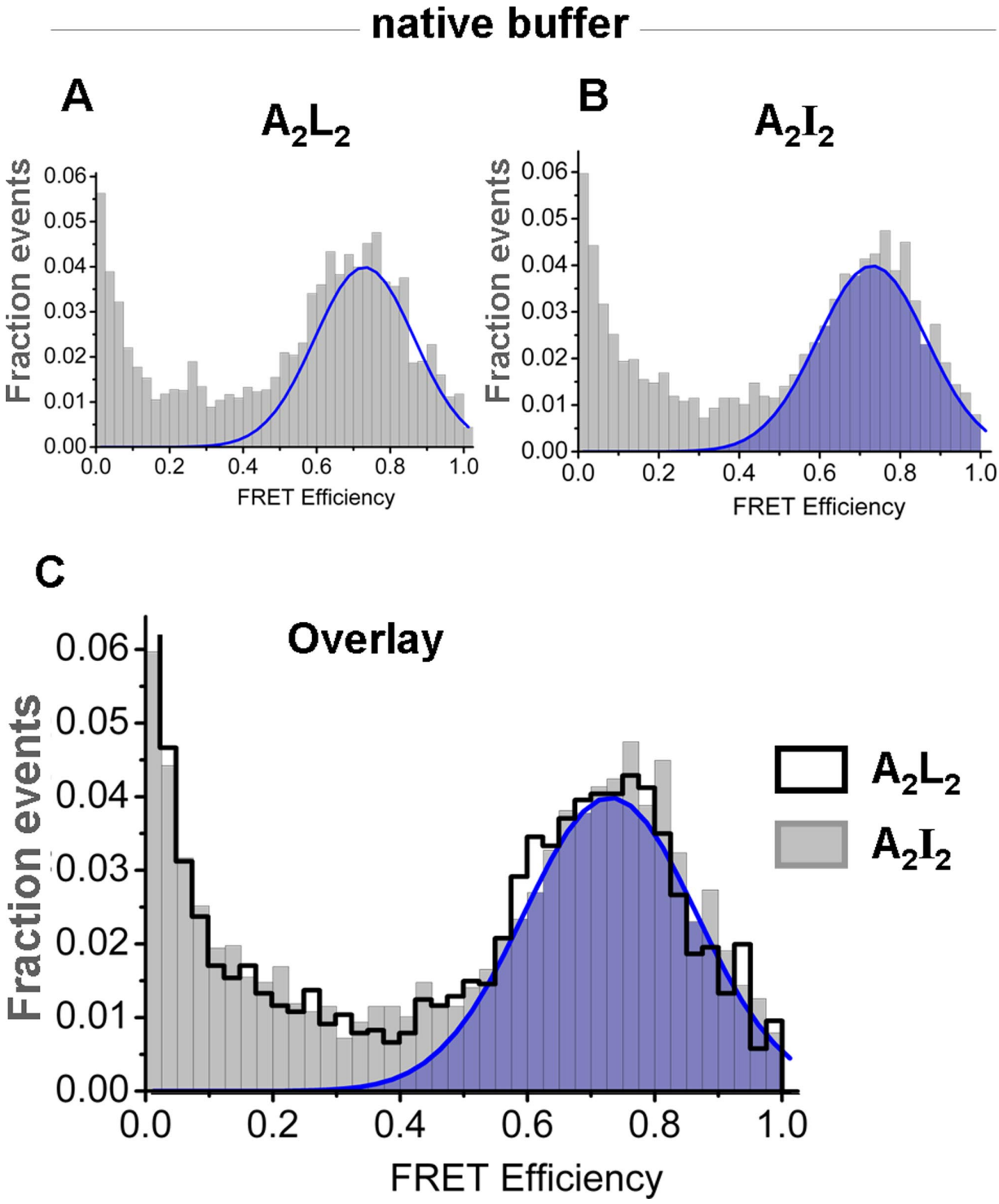

Fig. S3. Conformational balance for A_2L_2 probed by single-molecule FRET. In native buffer, the histogram obtained for A_2L_2 matches closely the one obtained for the reference A_2I_2.A_2L_2 and A_2I_2 have the same *syn* conformation in native buffer. Data measured for A_2L_2 at 0 M GdmCl (*A*) to the histogram obtained in the same conditions for A_2I_2 (*B*). (*C*) Overlay showing the similarity of the two histograms (A_2L_2, black line; A_2I_2, gray bars). The histogram obtained for A_2L_2 in slightly denaturing conditions (0.6 M GdmCl) displays two FRET peaks (Fig. S4*B*), each of which correlates well with the WT and A_2I_2 reference peaks (Fig. S4*A*,*C*). We therefore conclude that A_2L_2 is able to adopt both *anti* and *syn* conformations. Furthermore, to test that we indeed observe a mixture of *syn* and *anti* conformations for A_2L_2 at 0.6M, we mixed 50% WT and 50% A_2I_2 and observed a very similar histogram, showing a very similar occupation of *syn* and *anti* structures in the two cases (Fig. S4*D*).

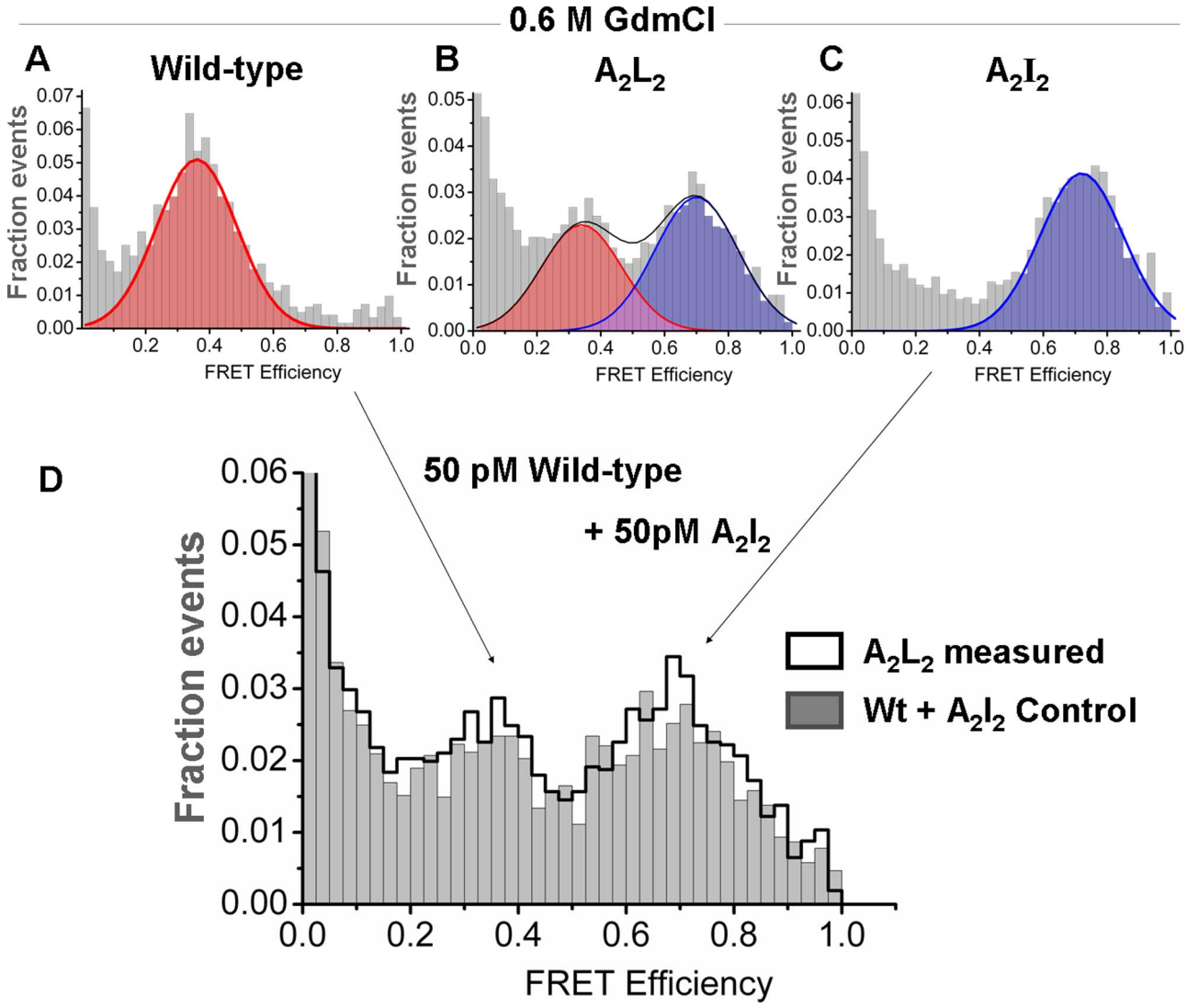

Fig. S4. Experimental control. A_2L_2 populates both *anti* and *syn* conformations under mild denaturation. (*A–C*) smFRET histograms obtained at 0.6 M GdmCl for WT, A_2L_2 and A_2I_2. (*D*) Overlay of the data observed for A_2L_2 (black line) and of a mixture of 50 pM WT + 50 pM A_2I_2 (gray bars). The two dimers were preformed in native buffer, measured separately then mixed in 0.6 M GdmCl, leading to a histogram that matches the one obtained for A_2L_2.

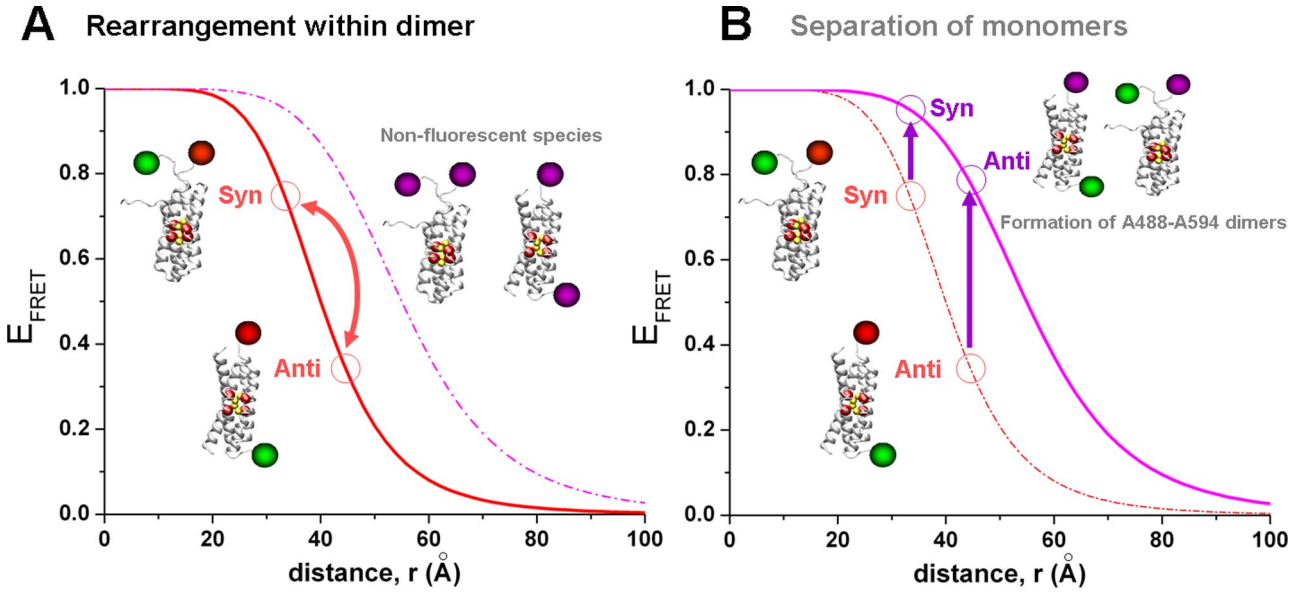

Fig. S5. Competition by monomers labeled with a second acceptor tests for dimer dissociation during conformational transitions. The 3-color experiments conducted in this work exploit the differences of distance-dependence of the FRET efficiencies between various FRET pairs. Especially, the A488-A647 and A488-A594 dye pairs have specific and well-separated Förster distances (R_0), which for a given donor-acceptor pair is the inter-dye distance for which $E_{FRET} = 0.5$. The red and purple lines in Fig. S5 shows the FRET efficiency as a function of interdye distance *r*,

$$E_{FRET} = \frac{1}{1 + \left(\frac{r}{R_0}\right)^6}$$

for the A488-A647 and A488-A594 dye pairs, calculated with R_0 values of 40 Å and 55Å respectively. As described in *A*, the slightly denaturing conditions trigger interconversion between *syn* and *anti* folding states for the A_2L_2 mutant. These two conformations can be separated thanks to the adequate R_0 value of the A488-A647 FRET pair. If monomers labeled with A488 were to separate and refold with the A594-monomers present in excess in the solution, novel FRET species would appear (*B*). As the Förster distance R_0 is greater for the A488-A594 pair, both the *syn* and *anti* states would have higher FRET efficiencies. Using the same two detection channels, these two conformations cannot be distinguished (as observed in Fig. 4*C*), but the resulting FRET peak with $E_{FRET} = 0.85$ is clearly separated from the original peaks obtained with the A488-A647 pair. Our experiment demonstrates simply that little exchange of monomers occur during the structural switch between *syn* and *anti* structures.